A&A 388, 326–334 (2002)
DOI: 10.1051/0004-6361:20020497

Astronomy & Astrophysics

Spatial distribution of emission in unidentified infrared bands from the Midcourse Space Experiment survey

S. K. Ghosh and D. K. Ojha

Tata Institute of Fundamental Research, Homi Bhabha Road, Mumbai (Bombay) 400 005, India

Received 23 January 2002 / Accepted 12 March 2002

Abstract. The Midcourse Space Experiment (MSX) has surveyed the Galactic plane in four infrared bands between 6 and 25 μm. Two of these bands cover several Unidentified Infrared emission Bands (*UIB*s). With the aim of extracting the spatial distribution of the *UIB* emission on a large scale, a scheme has been developed to model the MSX data with emission in the *UIB*s alongwith the underlying thermal continuum from the interstellar dust. In order to test this scheme, a sample of five Galactic compact H II regions (Sh-61, Sh-138, Sh-152, Sh-156, Sh-186; Zavagno & Ducci 2001) for which imaging data in some individual *UIB*s is available from ISOCAM measurements, has been studied. The results of this comparative study on a small angular scale are as follows: (i) the morphological details extracted from our scheme agree very well with those from the superior ISOCAM measurements; (ii) the integrated strength of *UIB*s extracted from the MSX database correlates extremely well with the sum of the strengths of individual *UIB*s measured from ISOCAM. This tight correlation is very encouraging and promises the potential of MSX database for the study of large-scale spatial distribution of *UIB* emission (and the carriers of *UIB*s) in the entire Galactic plane.

Key words. infrared: ISM – ISM: lines and bands – ISM: H II regions

1. Introduction

The near- to mid-infrared spectrum originating from the interstellar medium of the Galactic star-forming regions consists of various features in addition to a continuum. The continuum emission is attributed to the thermal emission from the interstellar dust component and almost all narrow emission lines have been identified with atomic nebular, molecular and other transitions originating from the interstellar gas component. In addition, several broader features have been detected which have been identified with features due to the solid state material of the dust (e.g. silicate absorption features at ∼10 and ∼18 μm etc.). There exists a class of broad emission features, sometimes called "Unidentified Infrared emission Bands" (*UIB*s; at 3.3, 6.2, 7.7, 8.6, 11.3, 12.7 μm), the identity of whose carriers and emission mechanisms are still a subject of active research. Some of these bands are widely believed to be characteristic of the bending and stretching modes of C=C and C–H bonds in aromatic molecules (e.g. fluorescent emission of Polycyclic Aromatic Hydrocarbons or PAHs; Leger & Puget 1984; Allamandolla et al. 1985). However, other contenders also exist in the literature (e.g. amorphous materials with aromatic hydrocarbon; Sakata et al. 1984; Borghesi et al. 1987). The study of large scale distribution of emission in the *UIB*s in the Galactic plane in general and selected star forming regions in particular would be important in understanding the details of their emission mechanism.

The recent Infrared Space Observatory (ISO) mission, in particular the imaging camera ISOCAM, has made it possible to study selected Galactic star forming regions in the *UIB*s. The ISOCAM instrument has several filters with the passbands selected to cover these *UIB*s (and also the neighbouring continuum) so that emission in these individual features can be measured very precisely. However, it is unreasonable to expect Galactic plane surveys in *UIB* emission using the ISOCAM, since its primary objective was to achieve the best possible (nearly diffraction limited) angular resolution in studies of individual astrophysical sources. As a result, the largest single image from ISOCAM covers $\sim 3' \times 3'$.

With the advent of the Midcourse Space Experiment (MSX), new possibilities have emerged. The SPIRIT III instrument onboard the MSX spacecraft has surveyed the entire Galactic Plane ($|b| < 5°$) in four mid infrared bands centered around 8.3, 12.13, 14.65 and 21.34 μm with an angular resolution $\sim 18''$ (Price et al. 2001). These four bands are referred to as A, C, D and E spectral bands of MSX respectively (the SPIRIT III instrument also has two additional narrower bands at 4.29 and 4.35 μm, called B_1 and

Send offprint requests to: S. K. Ghosh,
e-mail: swarna@tifr.res.in

B_2 bands). The usefulness of the MSX survey for the study of the diffuse interstellar medium and global characteristics has already been demonstrated (Cohen & Green 2001; Cohen 1999). The MSX band A includes the dominant *UIB* features at 6.2, 7.7 and 8.7 μm. Similarly, the MSX band C includes the *UIB* features at 11.3 and 12.7 μm.

While the ISOCAM provides imaging capability of selected regions in narrower spectral bands at higher angular resolution ($3''$ or $6''$) the MSX survey covers the entire Galactic plane in four broader bands (two of these covering several *UIB*s in addition to the continuum). Making use of this complementarity of ISOCAM vis a vis MSX, the following scheme has been explored to study large-scale emission in the *UIB*s in the Galaxy:

- Model each picture element of the MSX images with an integrated emission in *UIB* features superimposed on a gray body continuum spectrum under some reasonable assumptions. The best fit solution (for each pixel) provides a measure of the *UIB* emission locally.
- Test the reliability of the above scheme by comparing the results of some selected Galactic star forming regions that have been studied using the ISOCAM and whose emission in individual *UIB*s has been quantified (e.g. Zavagno & Ducci 2001).
- The comparison should cover not only qualitative aspects, (e.g. structural details/morphology), but also the quantitative correlation between the integrated estimate of *UIB* emission from our scheme and the ISOCAM results.

Section 2 describes the modelling scheme in detail, and Sect. 3 presents the results for the sample of six Galactic star forming regions using the MSX survey data. In Sect. 4, a comparison is made between our results and those from the ISOCAM by Zavagno & Ducci (2001). The conclusions are summarised in Sect. 5.

2. The scheme

The publicly-available MSX Galactic plane survey radiance images (Infrared Processing and Analysis Center at `http://irsa.ipac.caltech.edu/applications/MSX`) in the four bands at 8.3 (A), 12.1 (C), 14.7 (D) and 21.3 (E) μm are gridded in $6'' \times 6''$ pixels, although the true angular resolution is $\sim 18.3''$ (Price et al. 2001), with the unit of $\mathrm{W\,m^{-2}\,sr^{-1}}$. The zodiacal background has already been subtracted out from these MSX survey maps. The spectrum emitted from each pixel is assumed to be a combination of a thermal continuum (modified Planck function or gray body) and the total radiance due to the relevant *UIB* features within the MSX band.

$$R_i = r_i^{UIBs} + \int (1 - \mathrm{e}^{-\tau_\nu}) \times B_\nu(T) \times RSR_i(\nu)\,\mathrm{d}\nu \quad (1)$$

$i = A,\ C,\ D,\ E$

where R_i are the measured radiances in the MSX bands. $B_\nu(T)$ is the Planck function, and the term in parenthesis emulates the gray body spectrum emitted by the dust grains. τ_ν is the optical depth due to the interstellar dust component at the frequency ν. The functions $RSR_i(\nu)$ represent the normalized relative spectral responses of the four MSX bands (Egan et al. 1999).

Since the range of frequencies covered by the MSX bands is limited, we assume a power law dependence of the dust emissivity on frequency, viz.,

$$\tau_\nu = \tau_{10} \times \left(\frac{\nu}{\nu_{10}}\right)^{\beta}. \quad (2)$$

τ_{10} is the optical depth at 10 μm and ν_{10} the frequency corresponding to wavelength 10 μm. The value of β is a constant determined from the type of dust assumed. The effect of varying β is discussed later. The r_i^{UIBs} are the modelled total radiances in *UIB*s within the ith MSX band. Since there are no known *UIB*s within the bands D and E of MSX, $r_D^{UIBs} = 0$ and $r_E^{UIBs} = 0$. In addition, it has been assumed that the total radiance due to the *UIB*s in band C is proportional to that in band A, viz.,

$$r_C^{UIBs} = \alpha \times r_A^{UIBs}. \quad (3)$$

Here α is held fixed to a reasonable value (based on available observational data and understanding) for all pixels of all star forming regions studied, though the effect of changing the value of α will also be discussed later.

For each pixel on the sky with sufficient signal to noise ratio in each of the four MSX bands (implemented by map dynamic range cuts), we solve the set of four equations (Eq. (1)), for the three unknown variables viz., T, τ_{10} and r_A^{UIBs}. A non-linear chi-square minimization scheme based on the finite difference Levenberg-Marquardt algorithm has been used for this purpose. The integrals in Eq. (1) are evaluated numerically using a cautious adaptive Romberg extrapolation method. In order to ensure that the best solution obtained indeed corresponds to a global minimum of chi-square, the computations are repeated for 125 different sets of initial guesses comprising of 5 values each of T, τ_{10} and r_A^{UIBs}. The grid of initial guess values for these three variables have been selected to cover a wide range of physical situations (e.g. T ranging between 50 and 800 K; τ_{10} between 10^{-6} and 10^{-2}; r_A^{UIBs} between 10^{-7} and 10^{-3} $\mathrm{W\,m^{-2}\,sr^{-1}}$).

Invariably, the same solution is obtained starting from almost all different sets of initial guesses. The procedure is repeated for all pixels of the MSX map resulting in spatial distributions of these three physical variables. Here we extensively use the map of r_A^{UIBs}, that can be compared with the measurements from ISOCAM.

3. Results

3.1. Results from ISOCAM

3.1.1. Available results from the literature and sample selection

From the literature we have selected the work of Zavagno & Ducci (2001; hereafter ZD), which is based on ISOCAM

measurements, for detailed comparison with results from our scheme of extracting emission in *UIB*s from the MSX data. The reason for selecting ZD is that they have very uniformly studied (using same set of filters) a reasonable sample size comprising of five Galactic compact H II regions, viz., Sharpless(Sh)-61, Sh-138, Sh-152, Sh-156 and Sh-186. They studied the entire 3–12 μm wavelength range accessible through ISOCAM. The ZD sample of compact H II regions are bright in the IRAS 12 μm band and are known to be strong emitters of *UIB*s at 7.7, 8.6 and 11.3 μm but show no silicate absorption feature at 10 or 18 μm. In addition, they represent a sequence in equivalent stellar type of the main exciting star.

Results of ZD are based on imaging with the $3'' \times 3''$ pixel mode of ISOCAM covering $87'' \times 87''$ regions around Sh-61, Sh-152 & Sh-186 and $174'' \times 87''$ around Sh-138 & Sh-156. Based on images in $SW1$ (centre λ: 3.57 μm; λ range: 3.05–4.10 μm; Césarsky et al. 1996), $SW2$ (3.30; 3.20–3.40), $LW4$ (6.00; 5.50–6.50), $LW6$ (7.75; 7.00–8.50), $LW8$ (11.4; 10.7–12.0) filters and five selected wavelengths using the CVF, they have quantified the *UIB* fluxes (actually radiances) in the 3.3, 6.2, 7.7 and 11.2 μm features integrated over the mapped regions.

3.1.2. Our estimation of the 7.7 μm *UIB* feature emission

Using the publicly available ISOCAM data of the ZD sample sources (ISO Postcards from the ISO Data Archive for General Users; `http://www.iso.vilspa.esa.es`), we have extracted the spatial distribution of emission in the 7.7 μm *UIB* feature, using a method similar (but not identical) to ZD. First of all the underlying continuum at 7.7 μm was estimated from power law interpolation using the CVF images at 6.91 and 8.22 μm. Next, this continuum was subtracted from the $LW6$ image and the resulting emission was attributed to the 7.7 μm *UIB* (hereafter $UIB_{7.7}$ map). The resulting maps are presented and discussed in the next section.

3.2. Results obtained from the MSX survey

The MSX images of the five sources from ZD sample were processed following the scheme described above. The dust emissivity power law index β has been taken to be 1.0, which is commonly used in the literature for general interstellar grains in the mid infrared wavelength region relevant to the MSX bands (Scoville & Kwan 1976; Savage & Mathis 1979; Mathis 1990). However, other values of β have also been explored to ensure that the results obtained here are not sensitive to the choice of β, as discussed later.

3.2.1. Choice of α

The value of α represents the ratio of radiances in the *UIB*s within the passbands of MSX bands C and A (see Eq. (3)). These correspond to the features at 11.2 and 12.7 μm (in band C) and at 6.2, 7.7 and 8.6 μm (in band A). The value of α used here is based on the recent work by Verstraete et al. (2001) using the ISO-SWS. They studied the 2.4–25 μm spectra of three selected bright Galactic interstellar regions where dense molecular gas is illuminated by stellar radiation. Their wavelength range covers all the four MSX bands adequately. In addition, their choice of the three regions, viz., NGC 2023, Orion bar and M17-SW spans a wide range of excitation parameters (flux as well as hardness of the radiation field). The spectral resolution of the ISO-SWS measurements used by them was either 200 or 500, large enough to resolve individual *UIB*s. The average value of α for the above three regions, representing different physical conditions, has been estimated by us from Fig. 1 of Verstraete et al. (2001) to be 0.32 (with a very small dispersion). The effect of choosing different values of α have been studied by us, as is discussed later.

From the study of Verstraete et al. (2001) it is clear that the contribution of forbidden ionic lines and molecular rotational lines to the radiance within the MSX bands is negligible compared to the *UIB*s and the underlying continuum. Hence the presence of these narrow lines should not affect our scheme of extracting the radiance due to the *UIB*s from the MSX data.

3.2.2. Maps of extracted UIB radiance

The extent of the angular region considered around each target was determined by the available dynamic ranges in the four MSX bands (i.e. only pixels satisfying the dynamic range condition in each band were modelled). The usable dynamic range, UDR, for each band was defined from the frequency distribution of the radiance values, $f(R)$, in the corresponding map in the following manner: $UDR = R_{\rm max} \ / \ (R_{\rm median} + R^{-}_{1/2})$, where $R_{\rm max}$ is the brightest pixel value, $R_{\rm median}$ is the median value of R as determined from $f(R)$, and $R^{-}_{1/2}$ represents the brightness value satisfying $f(R^{-}_{1/2}) = f(R_{\rm median})/2$ and $R^{-}_{1/2} < R_{\rm median}$. For a purely Gaussian distribution, the above translates to using the brightest $\sim$15% pixels of the full sample. It may be noted here that any particular choice of dynamic range only changes the outer boundary of the region where our scheme is applied by either including or excluding these pixels, without affecting any numerical results for other pixels. The details of the dynamic range used for the five regions are presented in Table 1.

The resulting integrated *UIB* radiance maps extracted by us from the MSX data for Sh-61, Sh-138, Sh-152, Sh-156 and Sh-186 are displayed in Figs. 1 to 5 respectively as isophot contour plots. The sizes of these maps are selected based on the regions covered by the study of ZD. The peak *UIB* radiance values are also listed in Table 1.

Morphologically the extracted *UIB* radiance maps are very similar to the corresponding maps of thermal continuum emission from the dust grains, in general (at the scale of MSX resolution). However, there are differences

Table 1. Dynamic ranges of MSX maps and extracted peak UIB_A radiance.

Source	MSX Master	Usable Dynamic Range				Peak(UIB_A)
name	Plate Number	Band A	Band C	Band D	Band E	$\mathrm{W\,m^{-2}\,Sr^{-1}}$
Sh-61	GP027.0+1.5	41	20	25	40	7.74×10^{-5}
Sh-138	GP105.0+0.0	30	17	19	80	8.35×10^{-5}
Sh-152	GP109.5-1.5	52	26	27	39	5.82×10^{-5}
Sh-156	GP109.5+0.0	71	41	51	109	9.93×10^{-5}
Sh-186	GP124.5+0.0	15	7.7	5.7	8.5	1.70×10^{-5}

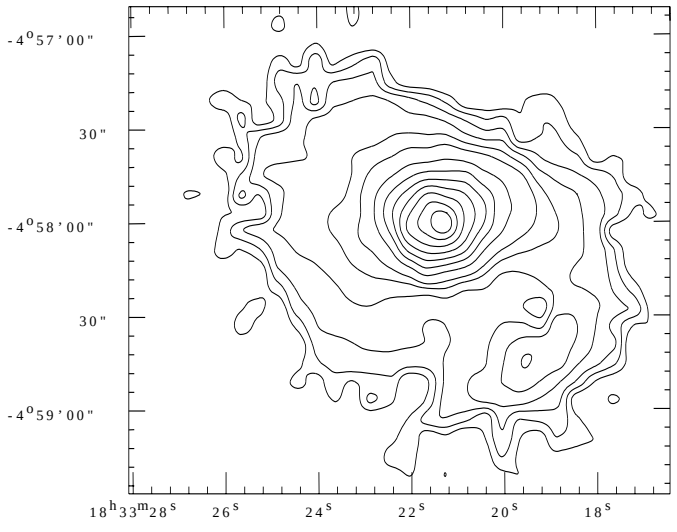

Fig. 1. The spatial distribution of total radiance in Unidentified Infrared emission Bands for the region around Sharpless 61, as extracted from the MSX maps. The contour levels are at 99, 90, 80, 70, 60, 50, 40, 30, 25, 20, 15, 10, and 5% of the peak value of 7.74×10^{-5} $\mathrm{W\,m^{-2}\,Sr^{-1}}$. The abscissa and the ordinate are RA (J2000.0) and Dec (J2000.0) respectively.

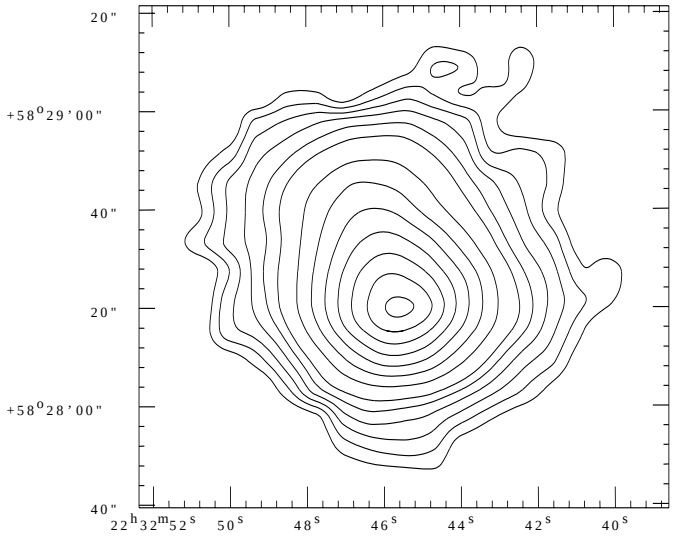

Fig. 2. Same as Fig. 1 but for the Sharpless 138 region. The contour levels represent the same fractions of the peak as in Fig. 1. The peak here is 8.35×10^{-5} $\mathrm{W\,m^{-2}\,Sr^{-1}}$.

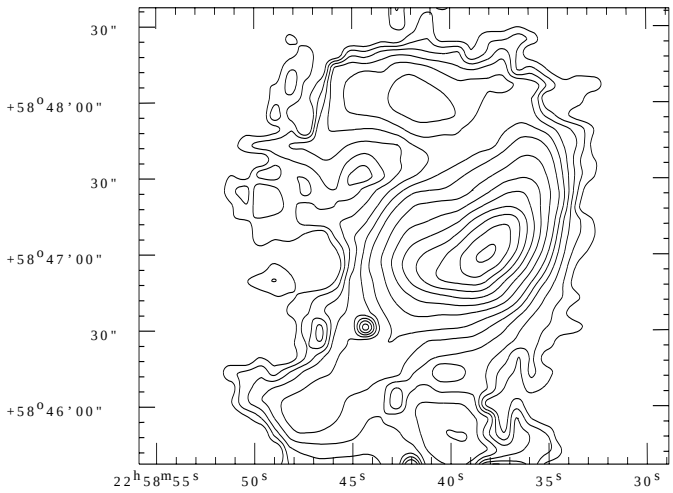

Fig. 3. Same as Fig. 1 but for the Sharpless 152 region. The peak here is 5.82×10^{-5} $\mathrm{W\,m^{-2}\,Sr^{-1}}$.

between the spatial distribution of *UIB* emission and the other modelled parameters, viz., the dust temperature and the optical depth corresponding to the thermal continuum emission. As one example, the map of dust optical depth (τ_{10}, at 10 μm) for the Sharpless 152 region is presented in Fig. 6, which can be compared with Fig. 3.

4. Comparison between MSX and ISOCAM results

4.1. Morphological similarities

It is instructive to compare our maps from modelling of MSX data with those based on the ISOCAM data. The most relevant ISOCAM filters for this comparison are $LW4$, $LW6$ and $LW8$ covering the 6.2, 7.7 and 11.2 μm *UIB*s. The former two features contribute to the *UIB* radiance in the MSX band A and the last one in the MSX band C.

The ISOCAM-based $UIB_{7.7}$ maps have been superimposed (grey scale) on our integrated *UIB* map extracted from MSX maps, viz. r_A^{UIBs}, (hereafter UIB_A), in Figs. 7 to 11 corresponding to Sh-61, Sh-138, Sh-152, Sh-156 and Sh-186 respectively. For a more general comparison involving other *UIB*s, we refer to Fig. 2 of ZD. In principle, our $UIB_{7.7}$ map for each source must resemble the $LW6$ map of ZD, which indeed is the case.

A marked morphological similarity between the contour plots corresponding to all these three ISOCAM

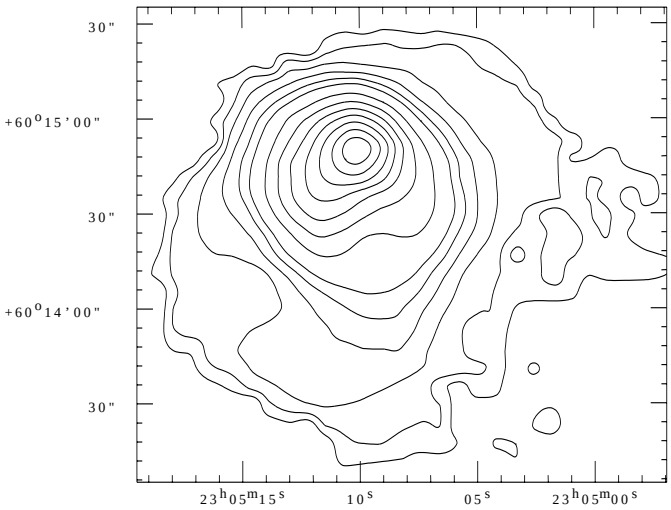

Fig. 4. Same as Fig. 1 but for the Sharpless 156 region. The peak here is 9.93×10^{-5} W m^{-2} Sr^{-1}.

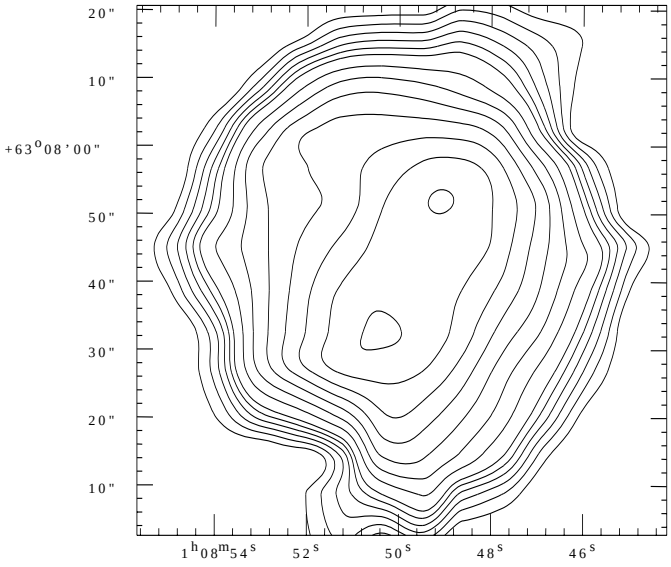

Fig. 5. Same as Fig. 1 but for the Sharpless 186 region. The peak here is 1.70×10^{-5} W m^{-2} Sr^{-1}.

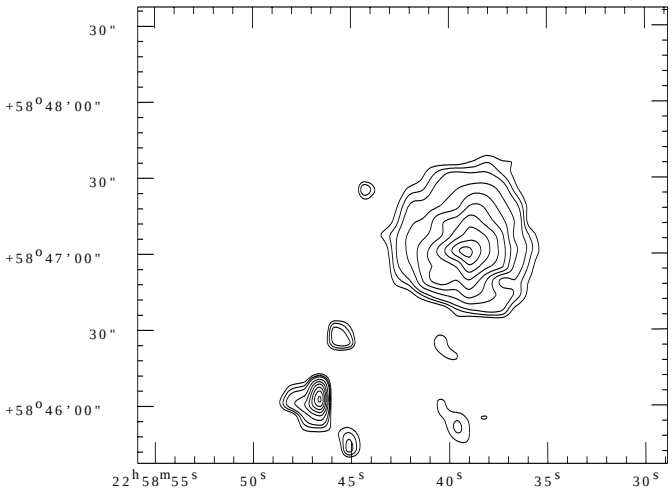

Fig. 6. The spatial distribution of dust optical depth (τ_{10} at 10 μm) for the Sharpless 152 region. The contour levels are at 99, 90, 80, 70, 60, 50, 40, 30, and 20% of the peak value of 3.49×10^{-4}. The structure of these contours differ from those of *UIB* radiance for the same region shown in Fig. 3.

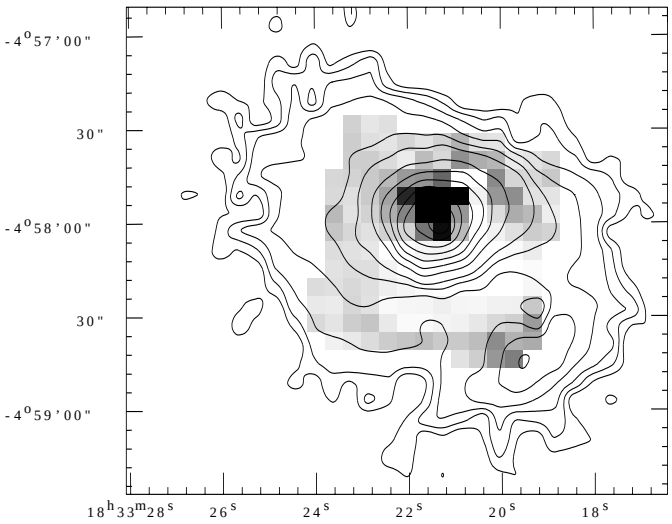

Fig. 7. Comparison of the total radiance in Unidentified Infrared emission Bands (UIB_A; contours, same as in Fig. 1) as extracted from the MSX maps, with the emission in the 7.7 μm *UIB* feature obtained from ISOCAM ($UIB_{7.7}$ in grey scale; the grey scaled region also represents the area imaged by ISOCAM), for the region around Sharpless 61. The abscissa and the ordinate are RA (J2000.0) and Dec (J2000.0) respectively.

filters ($LW4$, $LW6$, and $LW8$) for all the five sources support our assumption that r_C^{UIBs} and r_A^{UIBs} are correlated (Eq. (3)). Next, we comment qualitatively on structural similarities between the spatial distribution of emission in individual *UIB*s as obtained from ISOCAM (our $UIB_{7.7}$; $LW4$, $LW6$, and $LW8$ maps of ZD), vis-a-vis the total emission due to all *UIB*s within the MSX band A (UIB_A). Note that ZD's maps represent intensity while ours are radiance. For a qualitative comparison of structural details, it may be acceptable, however quantitive comparison is made in identical units later in this subsection.

4.1.1. Sharpless 61

The peak position for Sh-61 in the UIB_A map matches exactly that of $UIB_{7.7}$ (Fig. 7 here)/$LW6$ and $LW4$ (Fig. 2 of ZD). The general structure of the UIB_A contours is also very similar to the maps $LW4$, $LW6$ as well as $LW8$ of ZD, with extension along the E-W direction. We have detected an additional emission region S-W of the main peak in the UIB_A map, which is perhaps barely below the lowest contour displayed in $LW4$ or $LW6$. However, our $UIB_{7.7}$ map gives some hint of the same despite being near the edge of the ISOCAM field.

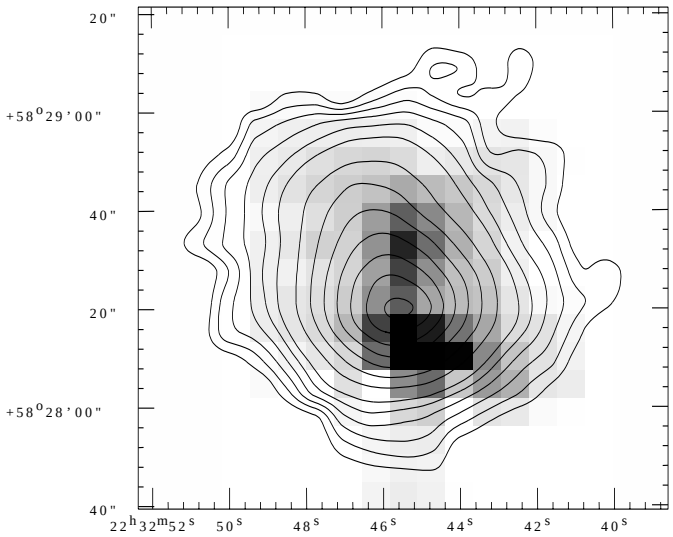

Fig. 8. Same as Fig. 7, but for the Sharpless 138 region.

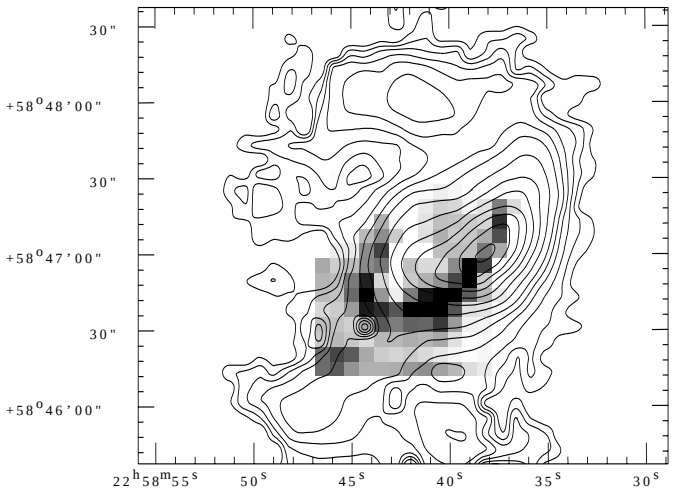

Fig. 9. Same as Fig. 7, but for the Sharpless 152 region.

4.1.2. Sharpless 138

For Sh-138 (Fig. 8), the $UIB_{7.7}$ map has been able to resolve two components along the N-S direction, and the UIB_A map shows the peak position as well as the contour shape consistent with them (note that the former has an angular resolution of $\sim 18''$ while ISOCAM's is $3''$). The contours in the $LW4$, $LW6$ and $LW8$ maps are remarkably similar with a main peak and extension towards the north.

4.1.3. Sharpless 152

Our $UIB_{7.7}$ (Fig. 9) as well as the $LW4$, $LW6$ and $LW8$ maps for Sh-152 show very rich (but again similar between these filters) structure at an angular scale beyond the scope of MSX's resolution. Still, our UIB_A map for Sh-152 reproduces the major structures consistent with the above, viz., the curved shape extending approximately from the S-E to N-W. The entire UIB_A map seems to be shifted by $\sim 10''$ with respect to the $UIB_{7.7}$ map. Additional interesting structures are detected in our map (see Fig. 3; due north and due south with respect to the main peak) that lie outside the region mapped by ISOCAM.

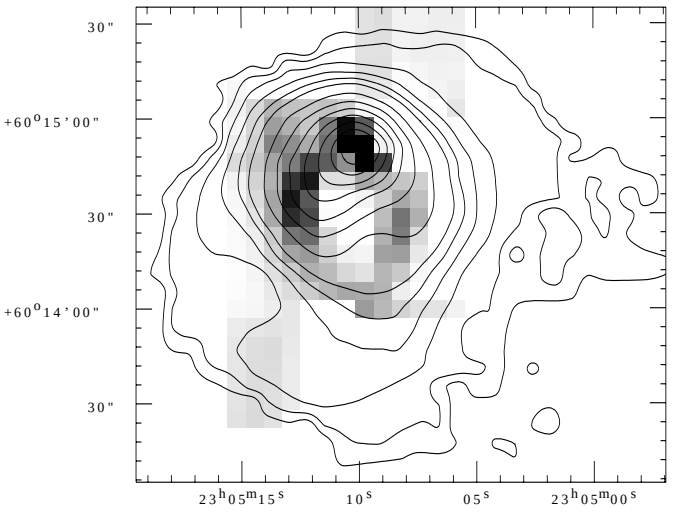

Fig. 10. Same as Fig. 7, but for the Sharpless 156 region.

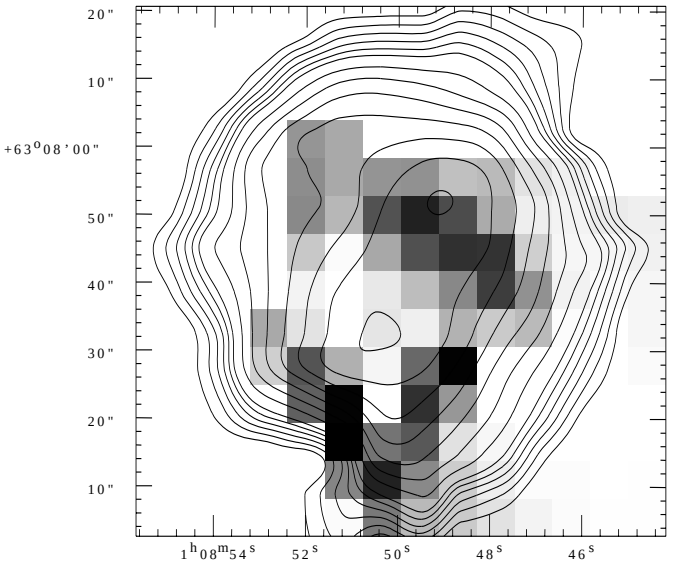

Fig. 11. Same as Fig. 7, but for the Sharpless 186 region.

4.1.4. Sharpless 156

In the case of Sh-156 the $UIB_{7.7}$, $LW4$, $LW6$ and $LW8$ maps also show structural details at a smaller angular scale that are unresolved in our UIB_A map (Fig. 10). However, the curvature and density of contours in the latter indicate a morphology consistent with the above ISOCAM maps. The positions of respective peaks match very well in all these maps. *UIB* emission is detected from a larger extended region all around the region mapped by ISOCAM, with one isolated secondary peak west of the main peak (Fig. 4).

4.1.5. Sharpless 186

The $UIB_{7.7}$ as well as the UIB_A maps have resolved the Sh-186 region into two major peaks separated mainly along the S-E to N-W line (Fig. 11). The stronger component is the S-E one in all maps. A similar structure is also seen in the $LW4$, $LW6$ and $LW8$ maps. The position of the peaks and other structural features also match very well (within $<10''$) between the UIB_A and all ISOCAM maps. The UIB_A map shows much more extended emission well outside the region mapped by ZD (Fig. 5).

4.2. Quantitative correlation

In order to make a quantitative comparison, the UIB_A radiance maps of the five regions have been integrated over the same corresponding regions as imaged by ZD, to get $I(UIB_A^{\rm MSX})$. ZD have tabulated the solid angle integrated *UIB* fluxes $F(3.3\ \mu{\rm m})$, $F(6.2\ \mu{\rm m})$, $F(7.7\ \mu{\rm m})$ and $F(11.2\ \mu{\rm m})$ in their Table 4. We have compared their $[F(6.2\ \mu{\rm m})+F(7.7\ \mu{\rm m})]= I({\rm ISOCAM}_{4+6})$ for each region with our integrated UIB_A radiances (see Table 2). Surprisingly, an extremely tight linear correlation has been found between $I({\rm ISOCAM}_{4+6})$ and $I(UIB_A^{\rm MSX})$. It has been found that the ratio, $\mathcal{R}_A = I(UIB_A^{\rm MSX})/I({\rm ISOCAM}_{4+6}) = 2.29 \pm 0.07$ (mean value and the error of the mean). This is despite several simplifying assumptions made in our analysis of the MSX data. This is indeed a remarkable finding, considering the very complex microscopic as well as macroscopic detail that must go into deciding the amount of emission in the *UIB*s. Whereas the *UIB*s at 3.3, 8.6, 11.3 and 12.7 μm originate from vibrational modes of the aromatic C–H bond, the bands at 6.2 and 7.7 μm arise from the aromatic C–C bonds. There is strong evidence from laboratory work on PAHs (carriers of *UIB*s), that the relative strengths of these features are very sensitive to the ionization state of the PAHs (Allamandola et al. 1999). Several observational studies of the spatial distribution of *UIB*s in well-resolved H II regions support this conclusion. Joblin et al. (1996) found that the ratio of 8.6 μm to 11.3 μm emission increases with the local far-UV (FUV) flux, which can ionize the PAH molecules. In a more recent study, Crété et al. (1999) found similar variations in the ratio of *UIB* features for the M 17 complex. One possible explanation for the above correlation is as follows: (i) the angular sizes of the sample of sources considered here are such that the intrinsic resolution of MSX ($\sim 18''$) spatially averages out various excitation effects expected close to the source of the FUV radiation field; and (ii) the sample spans a somewhat limited range of FUV luminosity ($\sim$2). It may be interesting to extend the present work to nearby star forming regions for which the MSX resolution is adequate to probe the *UIB* emitting regions close to the exciting FUV source, and also covering a larger range of $L_{\rm FUV}$.

In any case, our strong empirical correlation has many important and useful implications. For example, spatial distribution of emission in the *UIB*s for the entire Galactic plane can be studied following our method and the MSX survey with an angular resolution $\sim 20''$. Of course the ISOCAM data provides higher angular resolution information of selected regions and also the very important calibration factor above.

Since the band A of MSX includes the *UIB* at 8.6 μm in addition to the ones at 6.2 and 7.7 μm, it is natural to obtain a value for $\mathcal{R}_A$ greater than unity. The mean value of $\mathcal{R}_A$ so obtained can be interpreted in terms of the relative strength of the 8.6 μm feature vis-a-vis 6.2 μm + 7.7 μm features.

A similar correlation between UIB_C (which is just a scaled-down value of UIB_A) and the 11.2 μm feature emission measured using ISOCAM ($LW8$) by ZD has been explored for our sample of five sources. The ratio, $\mathcal{R}_C = I(UIB_C^{\rm MSX})/I({\rm ISOCAM}_8)$, turns out to be 2.98 ± 0.28, which shows a much larger dispersion. In view of the fact that band C of MSX also includes the *UIB* feature at 12.7 μm, the above is not surprising. The average value of $\mathcal{R}_C$ should provide information regarding the relative strengths of the features at 11.2 and 12.7 μm. The larger dispersion in the values of $\mathcal{R}_C$ among the five regions considered here is perhaps indicative of the observed variability of the strength of the 12.7 μm feature vis-a-vis other *UIB*s at shorter wavelengths (e.g. among the sources whose ISO-SWS spectra have been presented by Verstraete et al. 2001).

Next, we discuss how sensitive the value of $\mathcal{R}_A$ is to the various assumptions made in analysing/modelling the MSX data. One of the parameters while modelling the continuum from the MSX radiance in band A, is β, the dust emissivity index. Let us consider a few most popular types of dust grains, e.g., the Draine and Lee type (DL; Draine & Lee 1984), and Mathis, Mezger and Panagia (MMP; Mathis et al. 1983). One of the most popular dust size distribution is due to Mathis et al. (MRN; Mathis et al. 1977). The MRN size distribution averaged values of absorption cross sections for DL and MMP type dust, for silicate and graphite grains, have been computed (Mookerjea & Ghosh 1999; Mookerjea et al. 1999). Using these for the MSX bands A to E, we find the effective value of β to be in the range 0.56 to 0.89. All calculations were repeated for the values of $\beta = 0$ and 0.5 (in addition to 1.0). This had an insignificant effect on the value of $\mathcal{R}_A$, and also on the tightness of correlation between $I({\rm ISOCAM}_{4+6})$ and $I(UIB_A^{\rm MSX})$. It may be noted here that in the case where a strong silicate absorption feature at $\sim$9.8 μm was important, the above correlation could have been lost. The sample of ZD had been selected such that the silicate feature is not visible in the IRAS LRS spectrum.

Another very important parameter in our scheme is α (see Eq. (3)), which has been held at a value of 0.32 on the basis of the result of Verstraete et al. (2001). In order to study the sensitivity of our results on the numerical value of α, we have repeated the calculations for a range of its values between 0 and 0.7. We find that, for the value of α between 0.15 and 0.35, the correlation between $I({\rm ISOCAM}_{4+6})$ and $I(UIB_A^{\rm MSX})$ remains very

Table 2. Comparison of integrated radiances in *UIB*s obtained from ISOCAM measurements and those extracted by our scheme from MSX survey[a].

Source name	$I(\mathrm{ISOCAM}_{4+6})^b$ W.m^{-2}	$I(UIB_A^{\mathrm{MSX}})^c$ W m^{-2}	$\mathcal{R}_A$
Sh-61	1.64×10^{-12}	4.00×10^{-12}	2.44
Sh-138	1.50×10^{-12}	3.12×10^{-12}	2.08
Sh-152	1.74×10^{-12}	3.88×10^{-12}	2.23
Sh-156	2.20×10^{-12}	5.56×10^{-12}	2.53
Sh-186	3.83×10^{-13}	8.38×10^{-13}	2.19

[a] Solid angle integration has been carried out over an identical region in both cases (ISOCAM & MSX).
[b] From Zavagno & Ducci (2001).
[c] Extracted from the MSX Galactic Plane Survey data using the scheme presented here.

tight, though the numerical value of $\mathcal{R}_A$ changes slightly between 2.0 and 2.3. For values of α outside this range (0.15–0.35), the correlation becomes much poorer and also the value of $\mathcal{R}_A$ decreases on *either* side of this range. All of the above can be understood, if the total *UIB* feature strength in MSX bands A and C are really proportional. Hence we conclude that value of $\mathcal{R}_A$ determined here is physically meaningful and should help quantify the *UIB* emission in the Galactic plane in general.

5. Summary

A scheme has been developed to extract the contribution of Unidentified Infrared emission Bands (*UIB*s) from the mid infrared Galactic plane survey carried out by the SPIRIT III instrument onboard the Midcourse Space Experiment (MSX) satellite in four bands. The scheme models the observations with a combination of thermal emission (gray body) from interstellar dust and the *UIB* emission from the gas component, under reasonable assumptions. Thus the spatial distribution of emission in the *UIB*s with an angular resolution $\sim 20''$ (intrinsic to the MSX survey) has been extracted.

In order to verify the reliability of this scheme, a detailed comparison has been made with the results obtained by Zavagno & Ducci (2001) using the ISOCAM instrument onboard the Infrared Space Observatory (ISO), which has superior spectral and spatial resolution than that of the MSX survey. Five Galactic star forming regions, Sharpless 61 (Sh-61), Sh-138, Sh-152, Sh-156 and Sh-186, studied by Zavagno & Ducci (2001) have been used in this comparison.

The following results have been found:

- the *UIB* emission extracted from the MSX data is able to reproduce all major structural/morphological details detected by ISOCAM, consistent with its angular resolution;
- a very tight linear correlation has been found between the integrated *UIB* emission extracted from MSX data and that obtained from ISOCAM data (hence MSX-based *UIB* radiance estimates can be well calibrated); The above validates our assumption regarding the emissivity law for interstellar dust grains and is consistent with the assumed proportionality of *UIB* emission between the bands A and C of MSX. The correlation may be the result of spatial averaging over regions with different excitation details.
- the numerical value of the ratio of *UIB* radiances obtained from MSX and ISOCAM is important information for understanding the relative strengths of *UIB*s.

Hence, we conclude that our empirical scheme, along with the MSX Galactic plane survey, can be a powerful tool to study large-scale spatial distribution of *UIB* carriers.

Acknowledgements. It is a pleasure to thank the referee Dr. M. P. Egan whose suggestions have improved the scientific content of this paper. This research made use of data products from the Midcourse Space Experiment. Processing of the data was funded by the Ballistic Missile Defense Organization with additional support from the NASA Office of Space Science. This research has also made use of the NASA/ IPAC Infrared Science Archive, which is operated by the Jet Propulsion Laboratory, California Institute of Technology, under contract with the National Aeronautics and Space Administration.

The present work is based on observations with ISO, an ESA project with instruments funded by ESA Member States (especially the PI countries: France, Germany, The Netherlands and the UK) and with the participation of ISAS and NASA.

References

Allamandola, L. J., Hudgins, D. M., & Sandford, S. A. 1999, ApJ, 511, L115
Allamandola, L. J., Tielens, A. G. G. M., & Barker, J. R. 1985, ApJ, 290, L25
Borghesi, A., Bussoletti, E., & Colangeli, L. 1987, ApJ, 314, 422
Césarsky, C. J., Abergel, A., Agnese, P., et al. 1996, A&A, 315, L32
Cohen, M. 1999, in New Perspectives on the Interstellar Medium, ed. A. R. Taylor, T. L. Landecker, & G. Joncas, ASP Conf. Ser., 168, 97

Cohen, M., & Green, A. J. 2001, MNRAS, 325, 531
Crété, E., Giard, M., Joblin, C., et al. 1999, A&A, 352, 277
Draine, B. T., & Lee, H. M. 1984, ApJ, 285, 89
Egan, M. P., Price, S. D., Moshir, M. M., et al. 1999, MSX Point Source Catalog Explanatory Guide, AFRL-VS-TR-1999-1522
Joblin, C., Tielens, A. G. G. M., Geballe, T. R., & Wooden, D. H. 1996, ApJ, 460, L119
Leger, A., & Puget, J. L. 1984, A&A, 137, L5
Mathis, J. S. 1990, ARA&A, 28, 37
Mathis, J. S., Rumpl, W., & Nordsieck, K. H. 1977, ApJ, 217, 425
Mezger, P. G., Mathis, J. S., & Panagia, N. 1982, A&A, 105, 327
Mookerjea, B., & Ghosh, S. K. 1999, JA&A, 20, 1
Mookerjea, B., Ghosh, S. K., Karnik, A. D., et al. 1999, ApJ, 522, 285
Price, S. D., Egan, M. P., Carey, S. J., Mizuno, D. R., & Kuchar, T. A. 2001, AJ, 121, 2819
Sakata, A., Wada, S., Tanabe, T., & Onaka, T. 1984, ApJ, 287, L51
Savage, B. D., & Mathis, J. S. 1979, ARA&A, 17, 73
Scoville, N. Z., & Kwan, J. 1976, ApJ, 206, 718
Verstraete, L., Pech, C., Moutou, C., et al. 2001, A&A, 372, 981
Zavagno, A., & Ducci, V. 2001, A&A, 371, 312 (ZD)